Journal of Cerebral Blood Flow & Metabolism (2012) 32, 1948–1958

www.jcbfm.com

Dynamic study of blood–brain barrier closure after its disruption using ultrasound: a quantitative analysis

Benjamin Marty[1], Benoit Larrat[1,2], Maxime Van Landeghem[3], Caroline Robic[4], Philippe Robert[4], Marc Port[4], Denis Le Bihan[1], Mathieu Pernot[2], Mickael Tanter[2], Franck Lethimonnier[1] and Sébastien Mériaux[1]

[1]*NeuroSpin, I²BM, Commissariat à l'Énergie Atomique, Gif-sur-Yvette, France;* [2]*Institut Langevin, ESPCI ParisTech, CNRS UMR 7587, INSERM U979, Paris, France;* [3]*PPMD, ESPCI ParisTech, CNRS UMR 7615, Paris, France;* [4]*Guerbet Research Division, Roissy-Charles de Gaulle, France*

Delivery of therapeutic or diagnostic agents to the brain is majorly hindered by the blood–brain barrier (BBB). Recently, many studies have demonstrated local and transient disruption of the BBB using low power ultrasound sonication combined with intravascular microbubbles. However, BBB opening and closure mechanisms are poorly understood, especially the maximum gap that may be safely generated between endothelial cells and the duration of opening of the BBB. Here, we studied BBB opening and closure under magnetic resonance (MR) guidance in a rat model. First, MR contrast agents (CA) of different hydrodynamic diameters (1 to 65 nm) were employed to estimate the largest molecular size permissible across the cerebral tissues. Second, to estimate the duration of the BBB opening, the CA were injected at various times post-BBB disruption (12 minutes to 24 hours). A T_1 mapping strategy was developed to assess CA concentration at the ultrasound (US) focal point. Based on our experimental data and BBB closure modeling, a calibration curve was obtained to compute the half closure time as a function of CA hydrodynamic diameter. These findings and the model provide an invaluable basis for optimal design and delivery of nanoparticles to the brain.
Journal of Cerebral Blood Flow & Metabolism (2012) **32,** 1948–1958; doi:10.1038/jcbfm.2012.100; published online 18 July 2012

Keywords: BBB disruption; MR contrast agent; MRI; nanoparticles; T_1 mapping; ultrasound

Introduction

Cerebral tissues are isolated from circulating blood by the blood–brain barrier (BBB) (Rubin and Staddon, 1999). This physiological barrier consists of a lining of tightly packed vascular endothelial cells, different from the peripheral blood vessels (Hawkins and Davis, 2005). The tight junctions between these cells restrict the diffusion of microscopic objects (e.g., bacteria) and of large, hydrophilic molecules (>400 Da) from blood to brain parenchyma, while allowing the passage of small, hydrophobic molecules such as O_2, CO_2, proteins, and metabolites (Pardridge, 2005). Because of the neuroprotective nature of the BBB, delivery of potentially important diagnostic and therapeutic agents is a major challenge in the treatment of most brain disorders. Strategies to design specific drugs targeted to the brain involve finding an efficient mode of drug delivery across the BBB.

Recently, it has been demonstrated that the use of low power focused ultrasound combined with a systemic injection of lipid- (or polymer-) shelled microbubbles enables a noninvasive, local and transient disruption of the BBB (Hynynen *et al*, 2001). Many studies were then carried out to (1) establish optimal ultrasound parameters that permit adequate tissular penetration without causing tissue damage (Choi *et al*, 2006; Hynynen *et al*, 2005; O'Reilly *et al*, 2010, 2011*a*, *b*; Sheikov *et al*, 2008), (2) quantify permeability of the disrupted brain tissue (Vlachos *et al*, 2010, 2011), and (3) evaluate responses to treatments of particular brain disorders including tumors (Chen *et al*, 2010; Liu *et al*, 2010; Treat *et al*, 2008) and Alzheimer's disease (Jordao *et al*, 2010; Raymond *et al*, 2008). Most of these studies used magnetic resonance contrast agents (MR-CA) for monitoring the processes.

Despite a rapidly growing number of studies, the mechanism of ultrasound-induced BBB opening is understood only poorly. In particular, the maximum space that can be safely generated (ensuring reversibility) between endothelial cells, and the duration for

Correspondence: S Mériaux, PhD, CEA Saclay, DSV/I²BM/NeuroSpin, Bâtiment 145—Point courrier 156, 91191 Gif-Sur-Yvette Cedex, France.
E-mail: sebastien.meriaux@cea.fr
This study was supported by Iseult/Inumac French-German project.
Received 7 March 2012; revised 15 May 2012; accepted 11 June 2012; published online 18 July 2012

which this opening lasts, have not been measured. The knowledge of these parameters is crucial for the current development of brain targeted nanoparticles. Functionalized MR-CA for instance, are available in a wide range of hydrodynamic diameters: gadolinium (Gd) chelates, a few nm (Wadghiri *et al*, 2003), iron nanoparticles, 25 to 100 nm (Mendonca Dias and Lauterbur, 1986; Renshaw *et al*, 1986), gadolinium-based emulsions or liposomes, 200 to 300 nm (Devoisselle *et al*, 1988), and have very different vascular remanences, ranging from a few minutes to tens of hours. An estimate of the time window during which a molecule of a given size may be delivered across the BBB would be useful to monitor the amount of drug released to cerebral tissue and to adjust the dosage. For example, it has been shown that 3 to 8 nm wide particles are able to cross BBB 20 minutes after its ultrasound-induced disruption, but not particles of size 50 nm (Choi *et al*, 2010). Additionally, as the brain is unprotected while the BBB is open, it is important to know the time-to-recovery to limit any possible brain damages induced by tissular penetration of pathogenic agents.

The quantification of the amount of MR-CA crossing the BBB requires development of molecular imaging sequences via imaging techniques that are sensitive (high-field magnetic resonance imaging (MRI)) and provide outputs that can be correlated with the MR-CA concentration. Contrast agent quantification is one of the principal challenges for MR molecular imaging. Unlike other techniques such as fluorescence or nuclear imaging where the received signal comes directly from the CA, MR signal comes from the surrounding water protons and is therefore indirectly related to the presence of an exogenous probe. To quantify the CA concentration using MRI, it is necessary to model its interaction with the surrounding water molecules. Paramagnetic complexes interact with the surrounding water protons by decreasing their relaxation times (Swift and Connick, 1962). Contrast agent concentration can be linked to the T_1 or T_2 relaxation time decrease (in milliseconds). Here, we adapted a T_1 mapping sequence proposed by Deichmann and Haase (1992) and Deichmann *et al* (1999) that permitted estimation of a wide range of T_1 values with a good accuracy, and high spatial and temporal resolutions.

In this study, a calibrated BBB opening procedure was performed in healthy young adult rats under MR guidance. Five MR-CA were used (three paramagnetic and two superparamagnetic) with different hydrodynamic diameters (from 1 to 65 nm) to investigate the maximum permissible size of the gaps induced in the endothelial wall under safe conditions. Then, using the T_1 mapping strategy for the three paramagnetic CA, we quantified the amount of particles crossing the BBB when injected at different times after ultrasound-induced BBB disruption. This enabled quantitative monitoring of the dynamics of BBB closure for each given molecular size. Lastly, we present a theoretical model to fit the experimental data and derive a calibration curve to predict duration of BBB opening as a function of the hydrodynamic diameter of a given CA.

Materials and methods

Animal Preparation

All experiments were performed in accordance with the recommendations of the European Community (86/609/EEC) and the French legislation (decree no. 87/848) for use and care of laboratory animals. This study has been approved by the Comité d'ÉThique en Expérimentation Animale du Commissariat à l'Énergie Atomique et aux énergies alternatives Direction des Sciences du Vivant Ile de France (CETEA CEA DSV IdF) under protocol ID 12_009. A total of 47 Sprague Dawley male rats (80 to 100 g, Janvier, Le Genest-Saint-Isle, France) were used. Their head was shaved to ensure proper coupling of the ultrasound beam to the brain. Rats were anesthetized with 1.5% isoflurane in a mixture of air and oxygen, and placed in a cradle in prone position. A catheter (25 G needle) was positioned in the caudal vein to inject microbubbles and MR-CA from outside the scanner with minimal dead volume. Ten percent heparin was added to all injected solutions to avoid clot formation in the catheter. Body temperature and respiration rate were continuously monitored during the experiments.

Magnetic Resonance Contrast Agents

Magnetic resonance contrast agents of different hydrodynamic diameters were provided by Guerbet Research (Roissy-Charles de Gaulle, France). Main characteristics and injected doses of these nanoparticles are summarized in Table 1. After each MR-CA injection, the bolus was flushed by injection of 100 μL of saline solution. Three of the five MR-CA were paramagnetic Gd-chelates (Dotarem, P846, and P792) and were detected and quantified using T_1 strategies (Kang *et al*, 2010; Protti *et al*, 2010; Yankeelov *et al*, 2006). The other two CA (P904 and P03680) were ultrasmall superparamagnetic iron oxide (USPIO) nanoparticles. A T_2-weighted sequence was use to detect them in cerebral tissues (Hyodo *et al*, 2009; Philippens *et al*, 2004). Longitudinal r_1 and transverse r_2 relaxivities were measured *in vitro* at 7 T using galleries of tubes containing different concentrations of CA diluted in a 0.3% agar matrix, and maintained at 37 °C. For Gd-chelates, relaxivity values are in good agreement with those found in the literature (Fries *et al*, 2009).

Ultrasound Equipment

A MR-compatible focalized transducer (central frequency 1.5 MHz, diameter 30 mm, focal depth 20 mm, Imasonic, Voray sur I'Ognon, France) driven by a programmable function generator was used to produce ultrasound waves. It was coupled to the rat skull using a latex balloon filled with deionized and degassed water. Electrical power sent to the transducer was monitored during the BBB opening session. Main characteristics of the transducer (focal point size $0.6 \times 0.6 \times 3\,mm^3$, transcranial acoustic transmission

Table 1 Principal features of the paramagnetic and superparamagnetic nanoparticle contrast agents (CA) used in this study

	d_H (nm)	r_1 (mM^{-1}/s)	r_2 (mM^{-1}/s)	Dose (μmol/kg body weight)	Vascular remanence (minutes)	Diffusion coefficient ($\times 10^{-11}$ m^2/s)
Paramagnetic MR-CA						
Dotarem	<1	3.4	4.8	1500	26	4.6
P846	4	10.3	37	95	51	1.4
P792	7	4.9	42	210	32	0.8
Superparamagnetic MR-CA						
P904	21	1.4	88	1030	—	—
P03680	65	2.0	80	258	—	—

MR, magnetic resonance.
Hydrodynamic diameters (d_H) were measured by light scattering, longitudinal (r_1) and transverse (r_2) relaxivities were estimated at 7 T in 0.3% agar gels maintained at 37 °C, vascular remanences were taken from literature (Fries *et al*, 2009), and diffusion coefficients in brain parenchyma were estimated in a previous work (Marty *et al*, 2010). The paramagnetic CA were imaged using T_{1w}/T_1 mapping sequences, while the superparamagnetic using T_{2w} sequences.

factor 52% ± 5%) were estimated in a previous study (Larrat *et al*, 2010).

Blood–Brain Barrier Opening

Blood–brain barrier disruption was performed during MR imaging session thanks to a dedicated holder maintaining the ultrasound transducer above rat head. Its position was monitored using an ARFI (acoustic radiation force imaging) sequence and the right thalamus in the brain was chosen as a target for BBB disruption. Sonovue microbubbles (Bracco, Milan, Italy) were administrated via a bolus (1.5×10^8 bubbles/mL, 200 μL, 2 seconds) ~5 seconds before the beginning of ultrasound session. The bolus was flushed by injection of 100 μL of saline solution. Sonication was performed with 3 milliseconds bursts every 100 milliseconds for 1 minute (Choi *et al*, 2011). The peak-negative acoustic pressure at the ultrasound focal point was calibrated to 0.45 MPa, a level sufficiently low to ensure safe and reversible BBB opening (Larrat *et al*, 2011; Chopra *et al*, 2010). Anatomical images were acquired at the end of each MRI session to verify integrity of the brain tissues.

Magnetic Resonance Imaging Acquisitions

Magnetic resonance imaging was performed on a 7 T/90 mm Pharmascan scanner (Bruker, Ettlingen, Germany). A saddle coil was specially designed in-house for excitation and signal reception. The geometry and size of the resonator (diameter 30 mm) were optimized to maximize the overall signal-to-noise ratio over the whole brain while allowing the ultrasound beam to propagate from the transducer to the rat brain.

A multislice spin-echo sequence was modified to include additional motion-sensitizing gradients, and synchronized to ultrasonic bursts so that the phase signal was proportional to local acoustic intensity (Larrat *et al*, 2010; McDannold and Maier, 2008). This ARFI sequence was acquired with the following parameters: TE (echo time)/TR (repetition time) = 40/1,700 milliseconds, $T_{acq} = 4$ minutes, $R = 0.5 \times 0.5 \times 1\,mm^3$, duration of the motion encoding gradients = 13.3 milliseconds, duration of the sonication = 3 milliseconds.

A high spatial resolution T_2-weighted rapid acquisition with refocused echoes (RARE) sequence (TE_{eff}/TR = 32/4,200 milliseconds, $R = 0.125 \times 0.125 \times 0.3\,mm^3$) was used to detect the presence of USPIOs, and also for acquiring images at the end of every experiment to confirm lack of hemorrhages or edema due to ultrasound. T_1-weighted multi-slice multi-echo (MSME) sequence (TE/TR = 8/300 milliseconds, $R = 0.25 \times 0.25 \times 1\,mm^3$) was acquired to detect paramagnetic Gd-chelates.

To measure concentration of Gd-chelates, a T_1 mapping sequence was acquired before and after MR-CA injection. It consisted in a segmented series of FGE (fast gradient echo) images acquired at different time points after magnetization inversion to follow the entire T_1 recovery curve (Deichmann and Haase, 1992; Deichmann *et al*, 1999). Sequence parameters were: $TR_1 = 5$ milliseconds, TE = 2.5 milliseconds, 6 segments, 60 inversion times (from 64 to 5,800 milliseconds), flip angle = 5°, and $R = 0.2 \times 0.2 \times 1\,mm^3$. Repetition time between the acquisitions of two segments, TR_2, was 9 seconds, and total acquisition time was 12.5 minutes. A centric encoding of the *k*-space was chosen to avoid T_2 effects during echo trains at the acquisition of central lines.

Data Analysis

Data were analyzed using dedicated codes written in Matlab software (MathWorks, Natick, MA, USA). Maps of acoustic pressure index (IP_{ac}) were deduced from ARFI sequence using the following equation:

$$IP_{ac} \propto \frac{\sqrt{\varphi_{ON} - \varphi_{OFF}}}{P_{th}} \quad (1)$$

where φ_{ON} (respectively φ_{OFF}) is the phase of ARFI signal acquired with ultrasound (respectively without ultrasound), and P_{th} is the expected acoustic pressure at the focal point in case of an ideal ultrasound coupling. In a previous study (Larrat *et al*, 2010), we verified the linearity between acoustic intensity and MR-ARFI phase signal using the same setup. In another study (Larrat *et al*, 2011), we also characterized and verified the linearity between acoustic pressure and the amount of MR-CA crossing the BBB in the range of acoustic pressure values applied here.

To generate T_1 maps, the MRI signal measured with the FGE sequence was fitted as a function of the inversion time pixel by pixel as proposed by Deichmann and colleagues. Magnetic resonance contrast agents concentration maps (*C*) were then calculated from the $T_{1,0}$ map before MR-CA

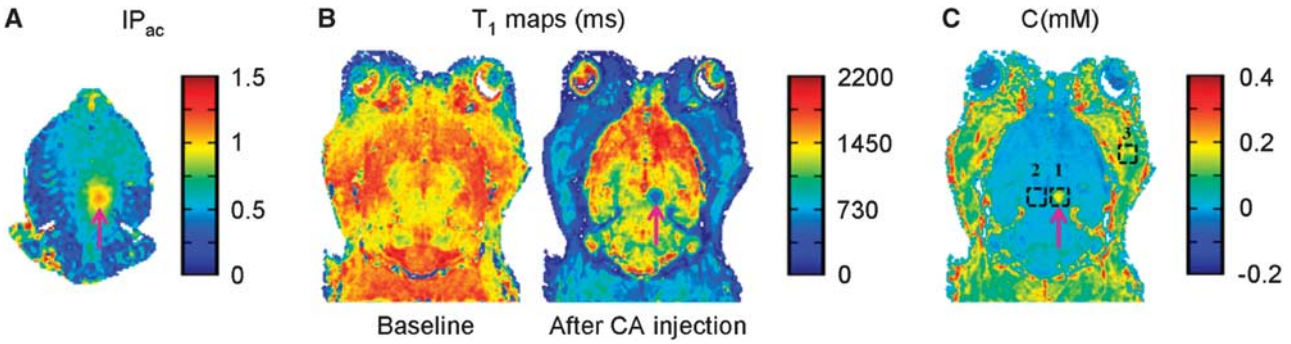

Figure 1 Different steps of magnetic resonance imaging (MRI)-guided ultrasound-induced disruption of blood–brain barrier (BBB). BBB disruption was achieved by intravenous injection of microbubbles via a catheter in the tail vein, in conjunction with transcranial ultrasound sonication. This was followed by injection of MRI contrast agent (CA) via the same catheter. The entire procedure was performed inside a 7 T MRI scanner. (**A**) Index of deposited acoustic pressure map derived from acoustic radiation force imaging (ARFI) images acquired before injection of microbubbles revealed the ultrasound focal point. (**B**) T_1 maps (in milliseconds) acquired before (Baseline) and after MR-CA injection. (**C**) MR-CA concentration map (in mM) derived from corresponding T_1 maps. Concentrations from three regions of interest (ROIs) were analyzed: ultrasound focal point ($n^\circ 1$), contralateral control region ($n^\circ 2$), and extracerebral control region in the cheek muscles ($n^\circ 3$).

injection and the T_1 maps after MR-CA injection using the following equation (Swift and Connick, 1962), considering that relaxivities r_1 measured *in vitro* in agar matrix hardly differ from the ones in rat brain tissues:

$$C = \frac{1}{r_1}\left(\frac{1}{T_1} - \frac{1}{T_{1,0}}\right) \quad (2)$$

Signals from different manually drawn ROIs (regions of interest) were analyzed. A ROI_{spot} of $0.6 \times 0.6 \times 3\,mm^3$ corresponding to the transducer focal point size was drawn in the right thalamus. To analyze the effect of BBB disruption, a similar ROI_{contra} was taken in the corresponding contralateral (left thalamus) region of the brain. This enabled correction for the residual vascular concentration of MR-CA during imaging. Another control ROI was drawn in an extracerebral region in the cheek muscles (ROI_{muscle}). For each rat, a corrected MR-CA concentration at the focal point (C^* without unit) was calculated as given below, based on the concentration measured at the ROI_{spot} ($C_{ROIspot}$), that at the control spots ($C_{ROIcontra}$ and $C_{ROImuscle}$), and the index of deposited acoustic pressure (IP_{ac}):

$$C^* = \frac{C_{ROIspot} - C_{ROIcontra}}{C_{ROImuscle}.IP_{ac}} \quad (3)$$

This processing step was mandatory to ensure the correction of the bias introduced by unequal injected volumes (unequal plasmatic concentrations) and the bias introduced by variations in acoustic wave penetration through the skull. These corrections allowed comparing MR-CA concentrations among animals.

Results

Low Power, Pulsed Ultrasound for Localized Disruption of Blood–Brain Barrier

In a rat model, BBB was opened transiently with the use of ultrasound, immediately followed by intravenous injection of Dotarem (Gd-chelate) and measurement of the amount of the MR-CA delivered across the BBB (Figure 1). Before the ultrasound sonication, ARFI was performed to obtain the acoustic pressure map in the brain (Figure 1A). This sequence was used to verify that the ultrasound beam was focused at the desired point in the right thalamus, and to estimate the acoustic pressure at this focal point before microbubbles injection, ensuring that the acoustic pressure remains below a predetermined safety threshold (Chopra *et al*, 2010; Larrat *et al*, 2011). Once the transducer was set at the desired position, Sonovue microbubbles were injected intravenously via a catheter positioned in the caudal vein, and the BBB was disrupted by pulsed sonication for 1 minute. Dotarem was then injected using the same catheter. To measure the concentration of Dotarem delivered, T_1 maps were acquired before and after MR-CA injection (Figure 1B). There was high tissue perfusion of the CA (strong T_1 decrease) in the cheek and neck muscles, but not in the brain tissue due to the BBB. As expected, the ultrasound focal point (purple arrow) was the only area of the brain exhibiting a strong T_1 decrease indicating BBB disruption. Based on T_1 mapping, CA concentration was obtained at the three selected ROIs: ultrasound focal point, ROI_{spot} ($n^\circ 1$), a control region contralateral to the ultrasound focal point, ROI_{contra} ($n^\circ 2$) and a region in cheek muscles ROI_{cheeks} ($n^\circ 3$) (Figure 1C).

Maximum Gap Between Endothelial Cells After Reversible Ultrasound-Induced Disruption of the Blood–Brain Barrier

To determine the size of gaps generated after ultrasound-induced disruption of the BBB, we chose five different MR-CA of varying hydrodynamic diameters (Table 1) and verified their passage across BBB at the ultrasound focal point. The CA were intravenously injected ($n = 4$ rats for Gd-chelates and $n = 2$ for iron oxide nanoparticles) directly after ultrasound-induced BBB disruption. T_1-weighted

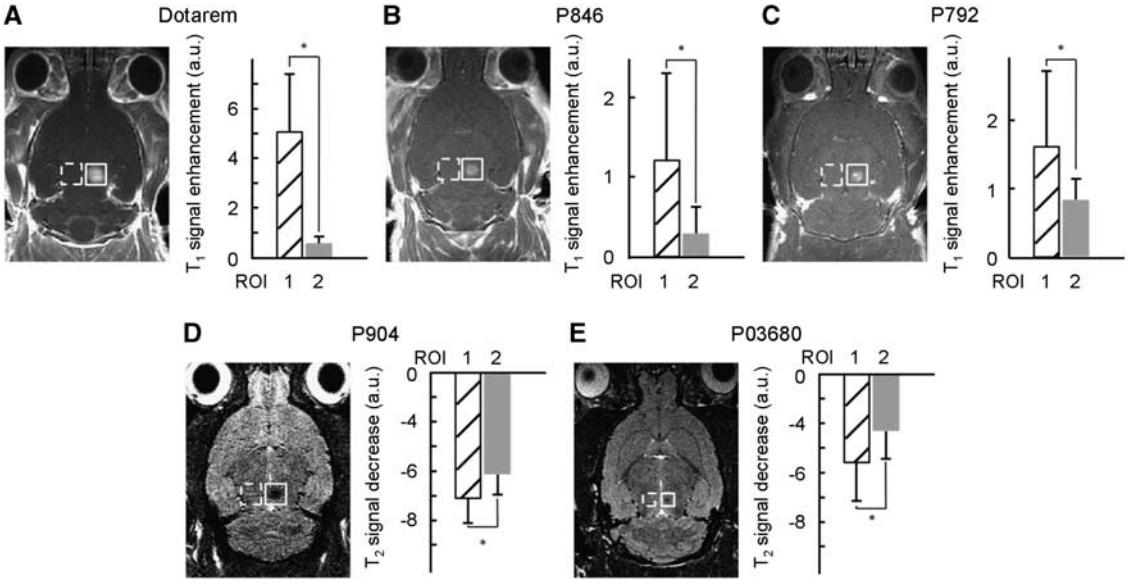

Figure 2 Ultrasound-induced localized delivery in rat brain of magnetic resonance imaging (MRI) contrast agents (CA) with different hydrodynamic diameters. Paramagnetic CA (Dotarem, P846 and P792) or ultrasmall superparamagnetic iron oxide (USPIO) CA (P904 and P03680) were injected in rats immediately after ultrasound-induced blood–brain barrier (BBB) disruption, and the signal intensities were measured within 5 minutes at the ultrasound focal point. T_{1w} images of the paramagnetic CA (**A**–**C**) revealed a positive contrast, while T_{2w} images of the USPIO revealed a negative contrast (**D**, **E**). Comparison of the signal enhancement in arbitrary units (a.u.) in the region of interest of ultrasound focal point (ROI_{spot}, $n°1$) and that in the control contralateral region (ROI_{contra}, $n°2$) is given next to the scan corresponding to each CA ($n = 1$ rat for each CA). The error bars correspond to the standard deviation observed within each ROI. Differences between the two regions were considered significant for P values < 0.01 (*) using a Student's t-test. ROI, region of interest.

(T_{1w}) images were obtained for the three paramagnetic CA and T_2-weighted (T_{2w}) images for the two USPIO CA (Figure 2). For all three Gd-chelates, a positive contrast was clearly visible on T_{1w} images at the ultrasound focal point, revealing the presence of the CA. Student's t-test performed on the measured MR signals confirmed that for each CA the difference between mean signals in ROI_{spot} and in ROI_{contra} was significant ($P<0.01$). For the 25-nm USPIO, a negative contrast appeared on T_{2w} images after its injection, suggesting that BBB was permeable to molecules of this size. Signal differences with contralateral region were also significant ($P<0.01$). However, the largest USPIO (65 nm) was detected only at the very focal point of the transducer as its penetration was significantly hindered compared with the smaller USPIO. The signal differences between ROI_{spot} and ROI_{contra} for this USPIO were not significant ($P>0.01$) if the ROI was of the standard size ($0.6 \times 0.6 \times 3\,mm^3$), but the differences became significant ($P<0.01$) if the size of the ROI_{spot} was decreased to $0.2 \times 0.2 \times 1\,mm^3$ around the focal point. These results suggest that 65 nm is close to the maximal gap between endothelial cells that is attainable after BBB disruption with this protocol.

Quantification of Magnetic Resonance Contrast Agent Concentration

Rats were injected with Dotarem at increasing doses (375, 750, and 1,500 μmol/kg, $n=1$ rat per dose) following BBB disruption. Concentration maps acquired by T_1 mapping were overlaid on the anatomical T_{2w} images (Figure 3A). Additionally, a T_1-weighted MSME sequence was also acquired. The estimated CA concentration at the ultrasound focal point was found to be proportional to the injected dose ($C_{375}<C_{750}<C_{1500}$) (Figure 3B). In contrast, the T_{1w} signals did not exhibit the same behavior and even saturated at high CA injected doses (Figure 3C). These observations confirm the high interest of our protocol to precisely quantify small variations of CA concentration, and that quantitative analysis based on T_{1w} signals alone can be misleading. Hence, results presented in the following sections of this study were all derived from quantitative data obtained using the T_1 mapping sequence (equation (3)).

Quantitative Study of Blood–Brain Barrier Closure Dynamics

The BBB closure dynamics was assessed using paramagnetic CA of different molecular sizes, administrated at different times after ultrasound-induced disruption. Rats were injected with the following CA: Dotarem ($n=10$ rats), P846 ($n=10$ rats), and P792 ($n=8$ rats) from 0 to 24 hours after ultrasound sonication. The reproducibility of CA delivery was verified by measuring both the injected dose and the acoustic power deposited at the ultrasound focal point. Contrast agent concentrations measured in the

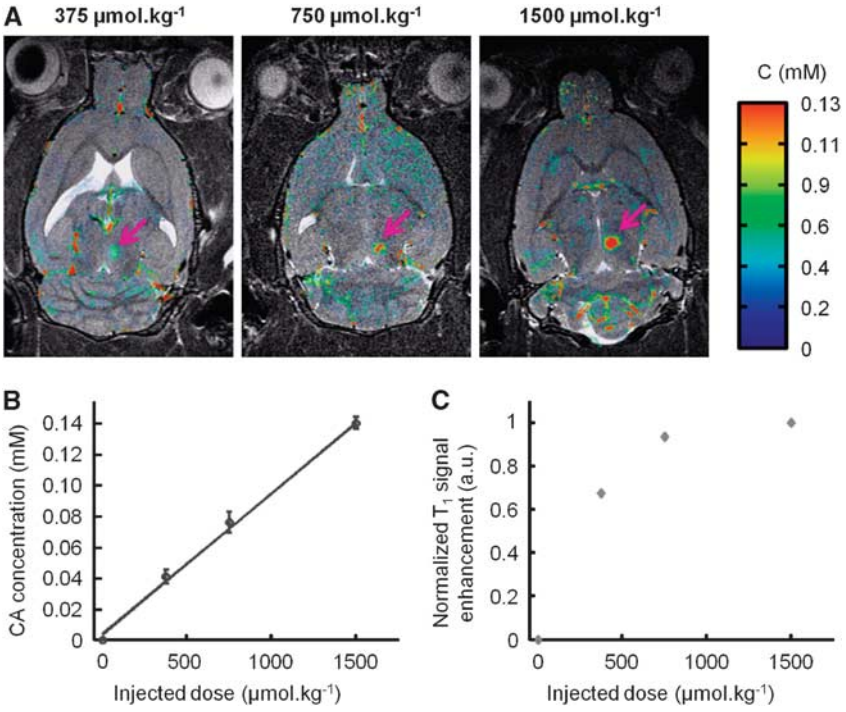

Figure 3 Comparison of T_1-weighted (T_{1w}) and T_1 mapping strategies to assess the amount of Gadolinium (Gd)-chelate crossing the blood–brain barrier (BBB). Dotarem was injected at different doses just after ultrasound-induced BBB disruption in the right thalamus, followed by the acquisition of one T_1 mapping sequence (to produce a concentration map) and one T_{1w} sequence. (**A**) Overlay of contrast agent (CA) concentration maps on the corresponding anatomical T_{2w} images after injection of increasing doses of Dotarem (375, 750, and 1,500 μmol/kg, $n = 1$ rat per dose). Purple arrows indicate the ultrasound focal spot where the BBB was disrupted. (**B**) CA concentration as estimated using T_1 mapping strategy at the ultrasound focal point showing linear dependence on the injected dose. The error bars correspond to the standard deviation observed within the regions of interest (ROI). (**C**) T_{1w} signal of the CA at the ultrasound focal point as a function of the injected dose showing a saturation effect.

cheek muscles in each animal were directly correlated with the injected dose since no permeability barrier like BBB exists in muscles (Figure 4A). Mean values were 0.345 ± 0.034 mM for Dotarem group, 0.061 ± 0.008 mM for P846 group and 0.040 ± 0.002 mM for P792 group. Variabilities observed within the above three groups (10%, 13%, and 5%, respectively) could be explained by experimental errors during injection and also by slight variations in the weight or metabolism of the animals. The index of the acoustic pressure (IP_{ac}) deposited at the focal point was estimated from ARFI sequence (Figure 4B) and was 1.13 ± 0.06 for Dotarem group, 1.00 ± 0.05 for P846 group and 0.97 ± 0.13 for P792 group. Variabilities observed within the above three groups (5%, 5%, and 13%, respectively) was mainly explained by slight differences in the placement of the transducer on the heads. Variations in the incidence angle of the ultrasound beam or in the thickness of the skull could have a significant impact on attenuation of the beam during its passage through the skull and lead to variations of the peak-negative acoustic pressure at the focal point.

Corrected CA concentrations (C^*) measured at the ultrasound focal point were plotted as a function of the time elapsed between BBB disruption and MR-CA injection (Figure 4C). For Dotarem (1 nm particle), the BBB was permeable for several hours post-BBB disruption. A significant amount of CA was detectable in the brain even when injected 8 or 9 hours after disruption. Around 24 hours after disruption, the BBB had apparently recovered its whole integrity, as very few CA were detectable in the brain tissues. P846 (4 nm particle) was delivered across the BBB only if injected within 2 hours post-BBB disruption. For P792 (7 nm particle), the duration of CA delivery to the brain was even shorter than for P846. One hour post-BBB disruption, the amount of CA crossing the BBB was about 30% of its initial value and dropped to undetectable levels after 90 minutes.

These findings confirmed that the duration of BBB crossing decreases when increasing CA hydrodynamic diameter. Second, it appears from the shape of the time-dependent concentration curve (Figure 4C) that the BBB permeability decreased at a faster rate initially and at a lesser rate later on.

A Model for Blood–Brain Barrier Closure Dynamics

Based on the experimental observations, the BBB closure dynamics was modeled as follows. First, it

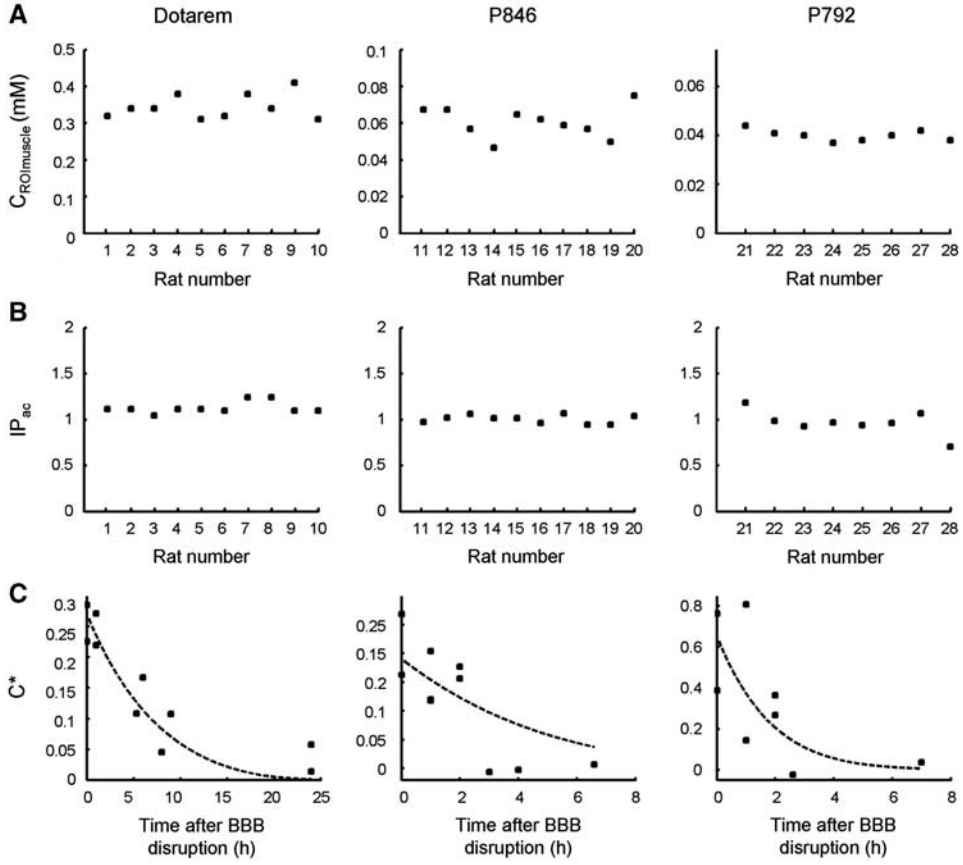

Figure 4 Blood–brain barrier (BBB) closure dynamics after ultrasound-induced disruption for magnetic resonance contrast agent (MR-CA) of different molecular sizes. Paramagnetic CA were injected at different times (0 to 24 hours) after BBB disruption. (**A**) Concentrations of the three paramagnetic CA in the region of interest in the cheek muscles $C_{ROImuscle}$ were measured. (**B**) Index of delivered acoustic pressure at the ultrasound focal point in the right thalamus in the brain. The maximum variability within each group (CA) for these two parameters was 13%. (**C**) Corrected concentration (C^*) of the CA at the ultrasound focal point in the brain was plotted as a function of the time elapsed between ultrasound-induced BBB opening and the MR-CA injection ($n = 1$ rat per time point). All experimental data ($n = 28$ rats) were used to fit the theoretical BBB closure model and determine the two parameters ($\sigma_0 = 1.54$ nm, $k = 1.54 \times 10^{-5}$ per second) (equation (6)); dashed lines correspond to the fitted data for each MR-CA. ROI, region of interest.

was assumed that each individual gap generated in the BBB by ultrasound returns to its equilibrium position (i.e., closed) as a harmonic oscillator damped by fluid friction. The gap diameter as a function of time was therefore expressed as $d(t) = d_0 e^{-kt}$, where d_0 is the gap diameter just after BBB disruption and k a time constant representative of individual gap closure speed.

Next, the initial size distribution of gaps was assumed to be a hemi-Gaussian function centered on 0 with a standard deviation σ_0. These two conditions imply a distribution of gap sizes as a function of time expressed as follows:

$$N(x,t) \propto \frac{1}{\sigma_0 e^{-kt}} e^{-\frac{x^2}{2\sigma_0^2 e^{-2kt}}} \quad (4)$$

For each time t, the amount $Q_{CA}(t)$ of CA with hydrodynamic diameter d_H crossing the BBB in a unit volume after disruption is proportional to the inflow flux only, since the outflow of CA from brain to blood is assumed to be negligible due to high concentration in the blood compartment. Assuming a hard sphere behavior for CA molecules, $Q_{CA}(t)$ can be expressed as follows:

$$Q_{CA}(t) \propto \int_{d_H}^{+\infty} N(x,t).\frac{x^2}{d_H} dx \quad (5)$$

The CA diffusion in the brain outside of the BBB disrupted region is also neglected since the CA tissular concentration is quantified within a few minutes after CA intravenous injection. A previous study from our team (Marty *et al*, 2010) showed that the Gd-chelates used in this study do not diffuse fast enough in the brain parenchyma to make this effect significant: for example, the diffusion coefficient of Dotarem (1 nm particle) was estimated around 46 $\mu m^2/s$ (Table 1).

Integration of equation (5) gives:

$$Q_{CA}(t) \propto \frac{\sigma_0^2 e^{-2kt}}{d_H} \times \left(\sqrt{\frac{\pi}{2}}\left(1-erf\left(\frac{d_H}{\sqrt{2}\sigma_0 e^{-kt}}\right)\right)+\frac{d_H}{\sigma_0 e^{-kt}} e^{-\frac{d_H^2}{2\sigma_0^2 e^{-2kt}}}\right) \quad (6)$$

All experimental data ($n = 28$ rats) were pooled to be fitted by this theoretical BBB closure model using a Levenberg–Marquart algorithm. A characteristic gap diameter $\sigma_0 = 1.54 \pm 0.04$ nm, and a BBB closure rate $k = 1.54 \pm 0.08 \times 10^{-5}$ per second were estimated. The Pearson correlation coefficient R was equal to 0.79, demonstrating that the experimental data were reasonably well fitted by the proposed theoretical model. A typical standard deviation of 10% was observed on experimental concentration measurements within all regions of interest around the ultrasound focal point. From this observation, the uncertainties on σ_0 and k estimations were assessed by Monte Carlo simulations on 10^6 datasets.

The half closure time ($t_{1/2}$) was then defined as the time after disruption when the concentration of CA crossing the BBB was 50% of the maximal concentration obtained immediately after disruption. $t_{1/2}$ was then calculated as the numerical solution of the following equation:

$$\frac{1}{2}\left(\sqrt{\frac{\pi}{2}}\left(1-erf\left(\frac{d_H}{\sqrt{2}\sigma_0}\right)\right)+\frac{d_H}{\sigma_0} e^{-\frac{d_H^2}{2\sigma_0^2}}\right) = e^{-2kt_{1/2}} \times \left(\sqrt{\frac{\pi}{2}}\left(1-erf\left(\frac{d_H}{\sqrt{2}\sigma_0 e^{-kt_{1/2}}}\right)\right)+\frac{d_H}{\sigma_0 e^{-kt_{1/2}}} e^{-\frac{d_H^2}{2\sigma_0^2 e^{-2kt_{1/2}}}}\right) \quad (7)$$

From the fitted parameters (σ_o and k), half closure times could be estimated as a function of hydrodynamic diameters of the molecules by numerically solving equation (7) (Figure 5, black circles). The calculated half closure time was ~5.5 hours for a 1-nm particle; ~1.5 hours for a 4-nm particle, and about 30 minutes for a 7-nm particle. The grey crosses in Figure 5 correspond to an experimental estimation of half closure time for each Gd-chelate: 5 hours for Dotarem, 1.75 hours for P846, and 1 hour for P792. These values were obtained from Figure 4C: a linear interpolation between data points was used to determine the time after which the concentration at the ultrasound focal point is equal to half its initial value. These experimentally estimated half closure times were in good agreement with the theoretical ones.

For larger molecules, half closure times were greatly reduced (around 3 minutes for a 25-nm particle and only few seconds for a 65-nm particle). These results match the qualitative results obtained with USPIOs (Figure 2). Therefore, to deliver a significant amount of larger molecular size CA across the BBB, their intravenous circulation should coincide with the end of ultrasound sonication.

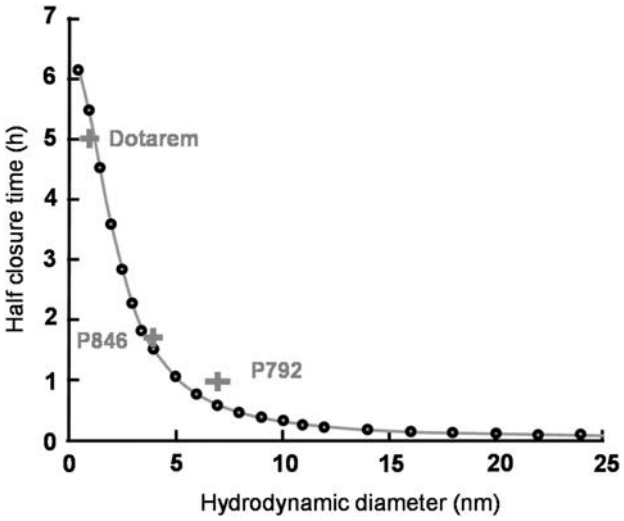

Figure 5 Prediction of the time window of blood–brain barrier (BBB) passage for a given nanoparticle size. Based on the theoretical model proposed here, half closure time, $t_{1/2}$ (the time after ultrasound-induced BBB disruption that is required for the delivery of 50% of the maximal dose to the predetermined ultrasound focal point in the brain) was calculated as a function of the hydrodynamic diameter of the nanoparticle (equation (7)) (black circles). Grey crosses correspond to experimental data on the paramagnetic nanoparticle contrast agents (CA) used here (Dotarem 1 nm; P846 4 nm; and P792 7 nm) and the solid line represents the best fit with analytical function: $t_{1/2} = A/(1 + B.d_H^2)$, where d_H is the hydrodynamic diameter of the injected CA (in nm) and A and B are constants, $A = 2.35 \times 10^4$ seconds and $B = 0.2106/nm^2$.

Lastly, it appears that the following analytical formula fits reasonably well the numerical solution of equation (7), enabling to directly estimate half closure time as a function of hydrodynamic diameter:

$$t_{1/2} = \frac{A}{1 + B.d_H^2} \quad (8)$$

with $A = 2.35 \times 10^4$ seconds and $B = 0.2106/nm^2$ (Figure 5, solid line).

Discussion

Ultrasound-Induced Blood–Brain Barrier Disruption

Drug delivery to the brain remains a major challenge for the treatment of most brain diseases. Although pathologies such as cancer degrade BBB integrity (Liu *et al*, 2012), it was proven that endothelial wall permeability is still poorer in these regions than in vessels of other organs. Recently, ultrasound-induced BBB disruption was demonstrated to be an effective method of significantly increasing permeability of the blood–tumor barrier in a controlled

manner (Chen *et al*, 2010). Another study reported that vessel wall permeability after ultrasound-induced BBB disruption was comparable to permeability values for unprotected organs (Vlachos *et al*, 2010). Our study further demonstrates that ultrasound combined with intravenous injection of microbubbles is a reliable, reproducible and non-invasive technique to deliver nanoparticles with hydrodynamic diameters up to 65 nm. Moreover, in our protocol, no edema or hemorrhages were detected on T_{2w} images following ultrasound sonication up to 24 hours after BBB disruption. Animals kept alive for several weeks after undergoing BBB disruption showed no adverse effects. The observation of a return to basal permeability within 24 hours for the smallest available CA (1 nm) further proved that the disruption was transient and reversible.

Magnetic Resonance Guidance

The ultrasound-induced BBB disruption described here was performed entirely under high-field MRI guidance. This is a challenge as it requires integrating a stereotactic frame, a MR-compatible ultrasound transducer adapted to the geometry of the rodent head and a dedicated RF (radiofrequency) coil into the 8.5-cm bore of a preclinical MRI scanner. The optimized RF coil allowed the quantification of Gd MR-CA at a micromolar range, with sufficient signal homogeneity over the whole brain and the ability for the ultrasound beam to propagate through the coil.

The anesthetized animal was placed inside the MRI scanner just before the start of the BBB disruption procedure till recovery. Thus, it was possible to obtain an acoustic intensity map before BBB disruption. This ensured a proper positioning of the ultrasound focal spot in the right thalamus and a precise *in situ* calibration of the acoustic pressure to avoid irreversible tissue damage. Furthermore, microbubbles were injected to cause ultrasound-induced BBB disruption followed by injection of MR-CA via the same catheter, which allowed imaging of the early events post-BBB disruption.

Maximum Gap Obtained Between Endothelial Cells

Contrast agents of increasing hydrodynamic sizes were tested, and the maximum gap width generated between endothelial cells after BBB disruption was estimated with our acoustic parameters. Gaps slightly above 65 nm could be generated safely, and the BBB recovered full integrity within 24 hours. The mechanical index of our setup was 0.37 which is below the standard value proposed by other studies for reversible BBB opening (McDannold *et al*, 2008). This result is particularly interesting from the view of development of targeted CA. Using a similar sonoporation protocol, it would be possible to deliver nanoparticles such as USPIOs, functionalized to target tissular biomarkers. In contrast, larger objects like emulsions or liposomes that typically have hydrodynamic diameters >100 nm, would be difficult to deliver to the brain using this technique, assuming a purely paracellular pathway. In general, an estimate of the maximum possible gap diameter would be helpful when the technique is applied to deliver therapeutic molecules. Several therapeutic drugs could benefit from this information: for instance, chemotherapeutic drugs such as Avastin ($d_H \sim 10$ nm), recombinant adeno-associated virus (rAAV) vectors for gene therapy ($d_H \sim 20$ nm), monoclonal antibodies such as anti-β-amyloid (d_H of few nm), and vectorized short interfering RNA used for gene expression modulation ($d_H \sim 50$ nm).

The maximum gap diameter measured in this study is probably dependent of the sonication parameters, in particular ultrasound frequency, pulse duration and duty cycle, total sonication time, and size distribution of injected microbubbles (Sonovue has a broad distribution between 1 and 8 μm). Here, we chose well-established parameters that have been proposed by others (Choi *et al*, 2011). Several groups have studied the influence of acoustic parameters (O'Reilly *et al*, 2011*a*) and microbubbles size (Samiotaki *et al*, 2011) on BBB opening. An optimization of parameters based on the knowledge gained from these studies may allow generation of pores larger than 65 nm wide.

Blood–Brain Barrier Closure Dynamics

In this study, the concentration of paramagnetic CA delivered at the ultrasound focal point was quantitatively measured, based on which, the duration of passage across the BBB was estimated for molecules of different sizes. This duration decreased rapidly as a function of hydrodynamic diameter of the CA. For instance, small molecules (around 1 nm) continued to cross the BBB for >10 hours, whereas large iron oxide particles (around 25 nm) had a time window of only a few minutes. Therefore, to maximize the amount of extravasation in the brain, large molecules should be injected right after or even during ultrasound sonication.

The results presented here also suggest a closure of the BBB at a progressively decreasing rate. We present a simple, damped, elastic model assuming an exponential decay of individual gap sizes to semi-quantitatively describe the observed dynamics of BBB closure. The experimental data were fed in the model to derive important physiological parameters, such as the typical closure time constant k that was estimated to be 1.54×10^{-5} per second. This parameter is an indirect measurement of the rate of endothelial cell relaxation after contraction. It could be used as a physio-pathological index of vessel integrity.

This model assumes a paracellular passage of injected molecules with an inflow limited by the size of the molecule relative to the size of the pores.

Our results support the notion that most of the crossing happens between endothelial cells rather than through them. This reinforces the hypothesis that during ultrasound-induced BBB opening, sonicated microbubbles exert a mechanical stress on endothelial cells, which makes them contract on themselves and loosen the junctions between them creating gaps (Vykhodtseva *et al*, 2008).

Limitations of the Study

The proposed BBB closure model has certain limitations. It does not take into account potential increased permeability of endothelial cell membranes (transcellular BBB crossing). It does not distinguish between hydrophilic and lipophilic molecules although it is known that lipophilic agents present an increased ability to cross the BBB via transcytosis (Pardridge, 2005). This concurrent release pathway could explain the observed differences between experimental data of P846 and P792 and predictions from the theoretical model.

The three Gd-chelates compared in this study have similar but not equal vascular remanences (Table 1). The tissular concentrations were measured within 12.5 minutes after CA injection, which is not a negligible time delay as the plasmatic half-life of the CA are between 26 and 51 minutes (Fries *et al*, 2009). Although during data processing the differences in overall injected plasmatic concentration were corrected for each CA (equation (3)), temporal variations of vascular concentrations during the T_1 mapping acquisition could be different from one CA to the other, none of them remaining strictly steady. The impact of these variations may be low since the MRI mapping acquisition was performed with a centric encoding scheme. Nevertheless, it may explain the differences between the theoretical model and the experimentally measured closure dynamics for the different molecules.

Conclusion

In this study, we developed a complete methodology for noninvasive, reversible and controlled ultrasound-induced BBB disruption under MR guidance that permitted precise quantification of the amount of MR-CA delivered to the brain parenchyma in a rat model. The two key parameters in designing drug delivery across the BBB, namely, the largest deliverable molecular size of the agent, and the time window for delivery of an agent of a given molecular size, were estimated for the first time.

Acknowledgements

The authors thank M Leopoldie for providing animal care, B Bresson for RF coil support, and Dr A Alahari for editing this manuscript.

Disclosure/conflict of interest

The authors declare no conflict of interest.

References

Chen PY, Liu HL, Hua MY, Yang HW, Huang CY, Chu PC, Lyu LA, Tseng IC, Feng LY, Tsai HC, Chen SM, Lu YJ, Wang JJ, Yen TC, Ma YH, Wu T, Chen JP, Chuang JI, Shin JW, Hsueh C, Wei KC (2010) Novel magnetic/ultrasound focusing system enhances nanoparticle drug delivery for glioma treatment. *Neuro-Oncology* 12:1050–60

Choi JJ, Selert K, Gao Z, Samiotaki G, Baseri B, Konofagou EE (2011) Noninvasive and localized blood-brain barrier disruption using focused ultrasound can be achieved at short pulse lengths and low pulse repetition frequencies. *J Cereb Blood Flow Metab* 31:725–37

Choi JJ, Small SA, Konofagou EE (2006) Optimization of blood-brain barrier opening in mice using focused ultrasound. IEEE Ultrasonics Symposium, Vancouver, Canada

Choi JJ, Wang S, Tung YS, Morrison III B, Konofagou EE (2010) Molecules of various pharmacologically-relevant sizes can cross the ultrasound-induced blood-brain barrier opening *in vivo*. *Ultrasound Med Biol* 36:58–67

Chopra R, Vykhodtseva N, Hynynen K (2010) Influence of exposure time and pressure amplitude on blood brain-barrier opening using transcranial ultrasound exposures). *ACS Chem Neurosci* 1:391–8

Deichmann R, Haase A (1992) Quantification of T1 values by Snapshot-Flash NMR imaging. *J Mag Reson* 96: 608–12

Deichmann R, Hahn D, Haase A (1999) Fast T1 mapping on a whole-body scanner. *Magn Reson Med* 42:206–9

Devoisselle JM, Viondury J, Galons JP, Confortgouny S, Coustaut D, Canioni P, Cozzone PJ (1988) Entrapment of gadolinium-DTPA in liposomes – characterization of vesicles by P-31 NMR-spectroscopy. *Invest Radiol* 23: 719–24

Fries P, Runge VM, Bucker A, Schurholz H, Reith W, Robert P, Jackson C, Lanz T, Schneider G (2009) Brain tumor enhancement in magnetic resonance imaging at 3 tesla intraindividual comparison of two high relaxivity macromolecular contrast media with a standard extracellular Gd-chelate in a rat brain tumor model. *Invest Radiol* 44:200–6

Hawkins BT, Davis TP (2005) The blood-brain barrier/ neurovascular unit in health and disease. *Pharmacol Rev* 57:173–85

Hynynen K, McDannold N, Sheikov NA, Jolesz FA, Vykhodtseva N (2005) Local and reversible blood-brain barrier disruption by noninvasive focused ultrasound at frequencies suitable for trans-skull sonications. *Neuroimage* 24:12–20

Hynynen K, McDannold N, Vykhodtseva N, Jolesz FA (2001) Noninvasive MR imaging-guided focal opening of the blood-brain barrier in rabbits. *Radiology* 220: 640–46

Hyodo F, Chandramouli GVR, Matsumoto S, Matsumoto K-I, Mitchell JB, Krishna MC, Munasinghe JP (2009) Estimation of tumor microvessel density by MRI using a blood pool contrast agent. *Int J Oncol* 35:797–804

Jordao JF, Ayala-Grosso CA, Markham K, Huang Y, Chopra R, McLaurin J, Hynynen K, Aubert I (2010) Antibodies targeted to the brain with image-guided focused ultrasound reduces amyloid-beta plaque load in the

TgCRND8 mouse model of Alzheimer's disease. *PloS One* 5:e10549

Kang CK, Park CA, Kim KN, Hong SM, Park CW, Kim YB, Cho ZH (2010) Non-invasive visualization of basilar artery perforators with 7T MR angiography. *J Magn Reson Imaging* 32:544–50

Larrat B, Marty B, Pernot M, Tanter M, Lethimonnier F, Mériaux S (2011) *MR-Acoustic Radiation Force Mapping Can Quantitatively Predict Drug Delivery Following Ultrasound-Induced Blood Brain Barrier Disruption in Rats at High Field*. Montreal, Canada: ISMRM

Larrat B, Pernot M, Aubry JF, Dervishi E, Sinkus R, Seilhean D, Marie Y, Boch AL, Fink M, Tanter M (2010) MR-guided transcranial brain HIFU in small animal models. *Phys Med Biol* 55:365–88

Liu HL, Hua MY, Chen PY, Chu PC, Pan CH, Yang HW, Huang CY, Wang JJ, Yen TC, Wei KC (2010) Blood-brain barrier disruption with focused ultrasound enhances delivery of chemotherapeutic drugs for glioblastoma treatment. *Radiology* 255:415–25

Liu HL, Yang HW, Hua MY, Wei KC (2012) Enhanced therapeutic agent delivery through magnetic resonance imaging-monitored focused ultrasound blood-brain barrier disruption for brain tumor treatment: an overview of the current preclinical status. *Neurosurg Focus* 32:E4

Marty B, Flament J, Giraudeau C, Robic C, Port M, Lethimonnier F, Boumezbeur F, Valette J, Le Bihan D, Mériaux S (2010) *Apparent Diffusion Coefficient of Gd-Based Contrast Agents Assessed in Vivo in the Rat Brain Using Dynamic T1 Mapping*. Stockholm, Sweden: ISMRM

McDannold N, Maier SE (2008) Magnetic resonance acoustic radiation force imaging. *Med Phys* 35:3748–58

McDannold N, Vykhodtseva N, Hynynen K (2008) Blood-brain barrier disruption induced by focused ultrasound and circulating preformed microbubbles appears to be characterized by the mechanical index. *Ultrasound Med Biol* 34:834–40

Mendonca Dias MH, Lauterbur PC (1986) Ferromagnetic particles as contrast agents for magnetic resonance imaging of liver and spleen. *Mag Reson Med* 3:328–30

O'Reilly MA, Huang Y, Hynynen K (2010) The impact of standing wave effects on transcranial focused ultrasound disruption of the blood-brain barrier in a rat model. *Phys Med Biol* 55:5251–67

O'Reilly MA, Waspe AC, Ganguly M, Hynynen K (2011*a*) Focused-Ultrasound disruption of the Blood-Brain Barrier using closely-timed short pulses: influence of sonication parameters and injection rate. *Ultrasound Med Biol* 37:587–94

O'Reilly MA, Yuexi H, Hynynen K (2011*b*) Standing waves in small animal models investigating ultrasound disruption of the blood-brain barrier. *AIP Conference Proceedings* 1359

Pardridge WM (2005) The blood-brain barrier: bottleneck in brain drug development. *NeuroRx* 2:3–14

Philippens MEP, Garnbarota G, Pikkemaat JA, Peeters WJM, van der Kogel AJ, Heerschap A (2004) Characterization of late radiation effects in the rat thoracolumbar spinal cord by MR imaging using USPIO. *MAGMA* 17: 303–12

Protti A, Sirker A, Shah AM, Botnar R (2010) Late gadolinium enhancement of acute myocardial infarction in mice at 7T: cine-FLASH versus inversion recovery. *J Magn Reson Imaging* 32:878–86

Raymond SB, Treat LH, Dewey JD, McDannold NJ, Hynynen K, Bacskai BJ (2008) Ultrasound enhanced delivery of molecular imaging and therapeutic agents in Alzheimer's disease mouse models. *Plos One* 3:e2175

Renshaw PF, Owen CS, McLaughlin AC, Frey TG, Leigh JS (1986) Ferromagnetic contrast agents – a new approach. *Magn Reson Med* 3:217–25

Rubin LL, Staddon JM (1999) The cell biology of the blood-brain barrier. *Ann Rev Neurosci* 22:11–28

Samiotaki G, Vlachos F, Tung Y-S, Konofagou EE (2011) A quantitative pressure and microbubble-size dependence study of focused ultrasound-induced blood-brain barrier opening reversibility *in vivo* using MRI. *Magn Reson Med* 67:769–77

Sheikov N, McDannold N, Sharma S, Hynynen K (2008) Effect of focused ultrasound applied with an ultrasound contrast agent on the tight junctional integrity of the brain microvascular endothelium. *Ultrasound Med Biol* 34:1093–104

Swift TJ, Connick RE (1962) NMR-relaxation mechanisms of 017 in aqueous solutions of paramagnetic cations and lifetime of water molecules in first coordination sphere. *J Chem Phys* 37:307–20

Treat LH, Zhang Y, McDannold N, Hynynen K (2008) *Impact of Focused Ultrasound-Enhanced Drug Delivery on Survival in Rats with Glioma*. Minneapolis, USA: ISTU

Vlachos F, Tung YS, Konofagou EE (2010) Permeability assessment of the focused ultrasound-induced blood-brain barrier opening using dynamic contrast-enhanced MRI. *Phys Med Biol* 55:5451–66

Vlachos F, Tung Y-S, Konofagou E (2011) Permeability dependence study of the focused ultrasound-induced blood-brain barrier opening at distinct pressures and microbubble diameters using DCE-MRI. *Magn Reson Med* 66:821–30

Vykhodtseva N, McDannold N, Hynynen K (2008) Progress and problems in the application of focused ultrasound for blood-brain barrier disruption. *Ultrasonics* 48: 279–96

Wadghiri YZ, Sigurdsson EM, Sadowski M, Elliott JI, Li YS, Scholtzova H, Tang CY, Aguinaldo G, Pappolla M, Duff K, Wisniewski T, Turnbull DH (2003) Detection of Alzheimer's amyloid in Transgenic mice using magnetic resonance microimaging. *Magn Reson Med* 50: 293–302

Yankeelov TE, DeBusk LM, Billheimer DD, Luci JJ, Lin PC, Price RR, Gore JC (2006) Repeatability of a reference region model for analysis of murine DCE-MRI data at 7T. *J Magn Reson Imaging* 24:1140–7